

## Development of $\text{MgFe}_2\text{O}_4$ as an oxygen carrier material for chemical looping hydrogen production

Jong Ha Hwang<sup>a</sup> and Ki-Tae Lee<sup>b,c,\*</sup>

<sup>a</sup>Department of Mineral Resources and Energy Engineering, Jeonbuk National University, Jeonbuk 54896, Republic of Korea

<sup>b</sup>Division of Advanced Materials Engineering, Jeonbuk National University, Jeonbuk 54896, Republic of Korea

<sup>c</sup>Hydrogen and Fuel Cell Research Center, Jeonbuk National University, Jeonbuk 54896, Republic of Korea

Chemical looping hydrogen production (CLHP) is an attractive technology for  $\text{H}_2$  production due to its ability to produce  $\text{H}_2$  and capture  $\text{CO}_2$  from fossil fuels simultaneously. In this paper, we present  $\text{MgFe}_2\text{O}_4$  as an oxygen carrier material with high efficiency, low cost, and stable properties for CLHP. The redox reactions occurred reversibly in the fuel, steam, and air reactor as  $\text{MgFe}_2\text{O}_4 \rightarrow \text{MgO/Fe}$ ,  $\text{MgO/Fe} \rightarrow \text{MgO/Fe}_3\text{O}_4$ , and  $\text{MgO/Fe}_3\text{O}_4 \rightarrow \text{MgFe}_2\text{O}_4$ , respectively. The oxygen transfer capacities of  $\text{MgFe}_2\text{O}_4$  for 5%  $\text{H}_2/\text{N}_2$  and 5%  $\text{CO}/\text{N}_2$  gases were about 23 wt% at 900 °C. Both the oxygen transfer capacity and rate were well maintained during 10 redox cycles at 900 °C. No phase changes or agglomeration occurred as the redox cycle number increased. Similarly,  $\text{MgFe}_2\text{O}_4$  did not exhibit significant degradation in its total amount or maximum rate of  $\text{H}_2$  production during four redox cycles. The average calculated amount of  $\text{H}_2$  production for  $\text{MgFe}_2\text{O}_4$  was 2,806 L/day per unit mass (kg).

**Keywords:** Chemical looping hydrogen production, oxygen carrier material, redox reaction, oxygen transfer capacity, oxygen transfer rate, attrition resistance.

### Introduction

The most important global issues in recent years are related to energy and the environment [1, 2]. In particular, there is a growing interest in the development of alternative energy sources with high efficiency due to the depletion of fossil fuels. Hydrogen, as a green and efficient energy source, is expected to play an important part in future energy systems, enhancing the feasibility of a hydrogen economy [3, 4]. Recently, many studies on hydrogen production through electrolysis of water using renewable energy, such as wind power and solar power, have been carried out; however, there are still many restrictions on commercialization because it is difficult to secure economic efficiency [5]. Alternatively, hydrogen production from fossil fuels is a way of reforming fuel; this can be done through the use of high-grade fuels (e.g., natural gas) and gasification of low-grade hydrocarbon fuels (e.g., coal and waste) [6, 7].

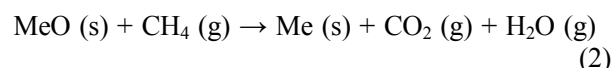
Global  $\text{CO}_2$  emissions also need to be reduced in the near future to mitigate global climate change. Therefore, various carbon capture and storage (CCS) technologies have been developed to reduce  $\text{CO}_2$  emissions [8]. There are a number of carbon capture technologies, which can be categorized generally into post-combustion

capture, pre-combustion capture, and oxy-combustion capture; these are the direct separation of  $\text{CO}_2$  from combustion flue gas,  $\text{CO}_2$  removal in the fuel conversion process prior to combustion, and the use of oxygen as the oxidant during fuel combustion generating a concentrated  $\text{CO}_2$  stream, respectively [9].

Chemical looping hydrogen production (CLHP) is a promising technology for hydrogen production because it can simultaneously produce  $\text{H}_2$  and capture  $\text{CO}_2$  from fossil fuels [10, 11]. The CLHP system consists of three reactors (i.e., an air reactor, fuel reactor, and steam reactor), and the oxygen carrier materials circulate and react with the reaction gas [12]. In an air reactor, the metal (Me) reacts with  $\text{O}_2$  in air to become a metal oxide (MeO) and unreacted air is discharged.



In the fuel reactor, fuel like  $\text{CH}_4$  reacts with a metal oxide (MeO). The metal oxide is reduced to metal (Me) and the fuel is burned to discharge  $\text{CO}_2$  and  $\text{H}_2\text{O}$ .



In the steam reactor, the metal (Me) reacts with  $\text{H}_2\text{O}$  to form a metal oxide (MeO).  $\text{H}_2$  and unreacted  $\text{H}_2\text{O}$  are discharged.



Based on the above reactions, the characteristics of CLHP technology are as follows.

\*Corresponding author:  
Tel : +82-63-270-2290  
Fax: +82-63-270-2386  
E-mail: ktlee71@jbnu.ac.kr

- Thermal NO<sub>x</sub> is not generated because a flame does not occur in the fuel reactor.
- In the fuel reactor, only CO<sub>2</sub> and H<sub>2</sub>O are discharged. Therefore, when H<sub>2</sub>O is condensed, a high concentration of CO<sub>2</sub> can be obtained.
- In the steam reactor, only H<sub>2</sub> and unreacted H<sub>2</sub>O are discharged; when H<sub>2</sub>O is condensed, a high concentration of H<sub>2</sub> can be obtained.
- The CO<sub>2</sub> separator and the H<sub>2</sub> separator are not needed; therefore, the process efficiency is high and the equipment cost can be reduced.

The metal oxide (MeO) that undergoes the redox reaction through the chemical looping process is called as an oxygen carrier material. Currently, the oxides of several transition metals, such as Ni, Fe, Cu, Mn, and Co, have been investigated intensively [13-15]. Among these various metal oxides, Fe-based oxygen carrier materials have the advantages of high oxygen transfer capacity, high melting temperature, low carbon deposition, low cost, and environmental friendliness [10, 11, 16]. However, several drawbacks, such as relatively low reactivity towards gaseous fuels and agglomeration that occurs during magnetite formation, may impede the application of Fe-based oxygen carrier materials [17]. Therefore, the development of innovative Fe-based oxygen carrier materials should focus on solving these issues. Several studies have reported that the NiFe<sub>2</sub>O<sub>4</sub> spinel phase formed from NiO-Fe<sub>2</sub>O<sub>3</sub> composites exhibited higher oxygen transfer capacities than individual NiO or Fe<sub>2</sub>O<sub>3</sub> [18, 19]. However, NiFe<sub>2</sub>O<sub>4</sub> still suffered from problems related to agglomeration.

In this paper, MgFe<sub>2</sub>O<sub>4</sub> spinel is proposed as an oxygen carrier material for CLHP for the first time. A reversible redox reaction between MgO/Fe and MgFe<sub>2</sub>O<sub>4</sub> can provide a relatively high oxygen transfer capacity. From this perspective, the phase analysis, redox mechanism, oxygen transfer properties, and H<sub>2</sub> production ability of an MgFe<sub>2</sub>O<sub>4</sub> oxygen carrier material for CLHP were systemically investigated in this study.

## Experimental Procedure

MgFe<sub>2</sub>O<sub>4</sub> powder was prepared by a conventional solid-state reaction method. Stoichiometric amounts of MgO (Alfa Aesar, UK) and Fe<sub>2</sub>O<sub>3</sub> (Alfa Aesar, UK) were mixed by ball-milling in ethanol for 48 h, followed by calcination in air at 1,200 °C for 3 h.

Phase analysis was carried out by X-ray diffraction analysis (XRD; MAX-2500, Rigaku, Japan) using a Cu K $\alpha$  radiation source. Diffraction patterns were recorded at a scan rate of 4°/min in the 2-theta range of 20 to 80°. The valence state of Fe in the sample was analyzed by X-ray photoelectron spectroscopy (XPS; AXIS Ultra DLD Kratos, UK) with monochromatic Al K $\alpha$ . Microstructures were observed using a field emission scanning electron microscope (FE-SEM; SN-300, Hitachi,

Japan).

The redox reaction of MgFe<sub>2</sub>O<sub>4</sub> in the CLHP process was evaluated by thermogravimetric analysis (TGA; TGA-N1000, Shinko, Korea) at 900 °C. 5% H<sub>2</sub>/N<sub>2</sub> or 5% CO/N<sub>2</sub> was utilized as the reducing gas and air was used as the oxidizing gas. The reducing and oxidizing gases were alternately flowed during the redox cycle experiment. Between the reducing and oxidizing gas flows, N<sub>2</sub> was purged for 5 min to prevent mixing of the reducing and oxidizing gases. The flow rate of each gas was 200 mL/min.

The H<sub>2</sub> production behavior of MgFe<sub>2</sub>O<sub>4</sub> during the redox cycle was analyzed by gas chromatography (GC; YL6100GC, Youngin, Korea). The temperature was raised to 900 °C at 10 °C/min in an Ar atmosphere and maintained for 12 h. 5% H<sub>2</sub>/Ar for reduction and 10% H<sub>2</sub>O/Ar for oxidation were alternately flowed for 1 h. Ar was purged between each reduction and oxidation step for 1 h.

## Results and Discussion

### Phase analysis and redox mechanism of MgFe<sub>2</sub>O<sub>4</sub>

The XRD patterns of MgFe<sub>2</sub>O<sub>4</sub> samples, both as-synthesized and after reaction with various reducing gases, are shown in Fig. 1. MgFe<sub>2</sub>O<sub>4</sub> powder synthesized at 1,200 °C for 3 h in air formed a single spinel phase without any impurities. MgFe<sub>2</sub>O<sub>4</sub> powders reduced in 5% H<sub>2</sub>/Ar and 5% CO/Ar at 900 °C for 1 h showed two phases with independent diffraction peaks of MgO and Fe. Alternatively, MgO and Fe<sub>3</sub>C were observed in the MgFe<sub>2</sub>O<sub>4</sub> powders reduced in 5% CH<sub>4</sub>/Ar at 900 °C for 1 h. In the case of CH<sub>4</sub>, carbon can be formed by a methane cracking reaction (CH<sub>4</sub> → C + 2H<sub>2</sub>) and react with Fe, resulting in the formation of Fe<sub>3</sub>C. In this regard, CO or syngas might be better than CH<sub>4</sub> as a fuel for MgFe<sub>2</sub>O<sub>4</sub>. Since the reduction of Fe<sub>2</sub>O<sub>3</sub> takes place

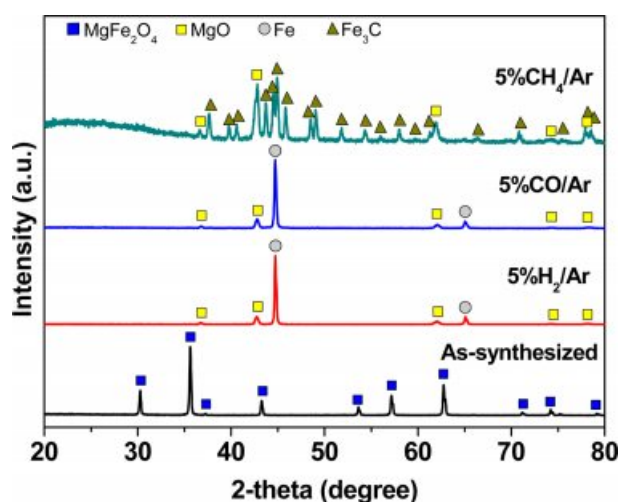


Fig. 1. XRD patterns of the as-synthesized MgFe<sub>2</sub>O<sub>4</sub> and samples reduced by various reducing gases at 900 °C for 1 h.

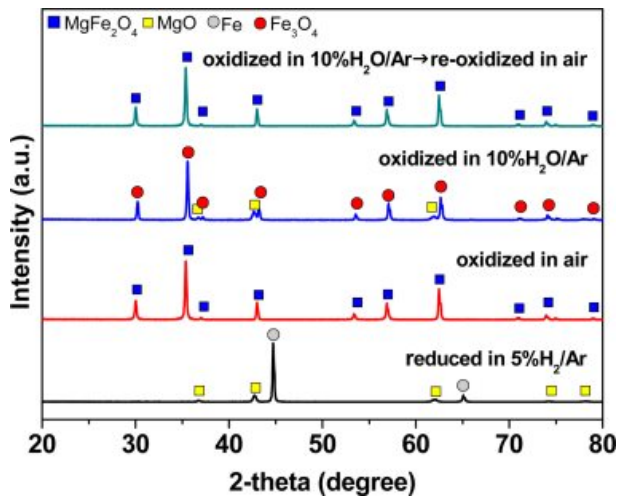


Fig. 2. XRD patterns of MgFe<sub>2</sub>O<sub>4</sub> according to the redox reaction at 900 °C for 1 h.

as a stepwise process [15], the reduction pathway of MgFe<sub>2</sub>O<sub>4</sub> can be suggested: MgFe<sub>2</sub>O<sub>4</sub> → MgO/Fe<sub>2</sub>O<sub>3</sub> → MgO/Fe<sub>3</sub>O<sub>4</sub> → MgO/FeO → MgO/Fe.

In order to confirm the redox mechanism of MgFe<sub>2</sub>O<sub>4</sub>, phase analysis was carried out after reduction in 5% H<sub>2</sub>/Ar followed by oxidation in air or 10% H<sub>2</sub>O/Ar. MgO and Fe, which are the reduced products of MgFe<sub>2</sub>O<sub>4</sub> in a 5% H<sub>2</sub>/Ar atmosphere, formed a single phase of MgFe<sub>2</sub>O<sub>4</sub> after oxidation in air, as shown in Fig. 2. On the contrary, the samples oxidized by 10% H<sub>2</sub>O/Ar existed in two phases, i.e., MgO and Fe<sub>3</sub>O<sub>4</sub>, rather than a single phase of MgFe<sub>2</sub>O<sub>4</sub>. It has also been reported that Fe could only be oxidized to Fe<sub>3</sub>O<sub>4</sub> under steam [20, 21]. However, when the sample oxidized in 10% H<sub>2</sub>O/Ar was re-oxidized by air, a single phase of MgFe<sub>2</sub>O<sub>4</sub> formed, as shown in Fig. 2.

XPS analysis was also carried out in order to confirm the valence state of Fe in MgFe<sub>2</sub>O<sub>4</sub> before and after the oxidation reaction at 900 °C for 1 h. The XPS spectra obtained for the various atmospheres are shown in Fig. 3. The binding energies of Fe 2p<sub>3/2</sub> and Fe 2p<sub>1/2</sub> in Fe<sub>2</sub>O<sub>3</sub> are 711.0 and 724.6 eV, respectively [22]. In the case of Fe<sub>3</sub>O<sub>4</sub>, the peak positions of Fe 2p<sub>3/2</sub> and Fe 2p<sub>1/2</sub> shift to lower binding energies of 710.56 and 724.07 eV, respectively [22]. The binding energies of Fe 2p<sub>3/2</sub> and Fe 2p<sub>1/2</sub> in MgFe<sub>2</sub>O<sub>4</sub> in this study were 710.8 and 724.4 eV, respectively, which indicates that the valence state of Fe in MgFe<sub>2</sub>O<sub>4</sub> is 3<sup>+</sup>. Alternatively, the binding energies of Fe 2p<sub>3/2</sub> and Fe 2p<sub>1/2</sub> in the sample oxidized in 10% H<sub>2</sub>O/Ar were shifted to lower binding energies of 709.9 and 723.4 eV, respectively. These results correspond to the peak positions of Fe<sub>3</sub>O<sub>4</sub>, indicating that the valence state of Fe in the sample oxidized in 10% H<sub>2</sub>O/Ar is a mix of 2<sup>+</sup> and 3<sup>+</sup>. Interestingly, the peak positions of Fe 2p<sub>3/2</sub> and Fe 2p<sub>1/2</sub> in the sample re-oxidized in air are identical to those of MgFe<sub>2</sub>O<sub>4</sub>.

Based on the phase analysis and the XPS results, we

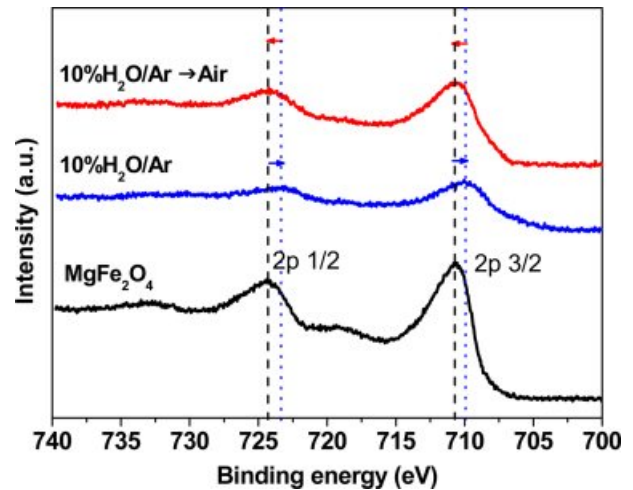
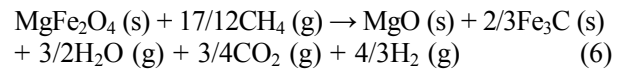
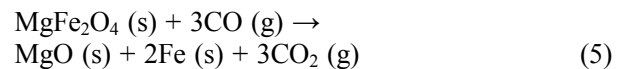
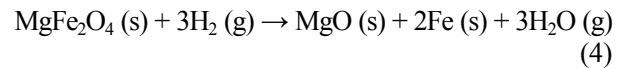
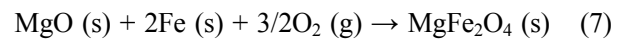


Fig. 3. XPS spectra of MgFe<sub>2</sub>O<sub>4</sub> before and after the oxidation reaction at 900 °C for 1 h.

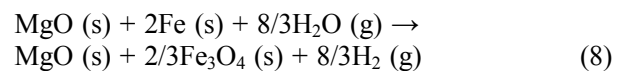
can confirm the redox mechanism of MgFe<sub>2</sub>O<sub>4</sub> at 900 °C. The reduction reactions of MgFe<sub>2</sub>O<sub>4</sub> with various gases in the fuel reactor can be described as follows.



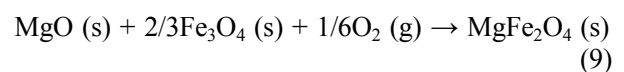
When the reduced MgFe<sub>2</sub>O<sub>4</sub> (MgO/Fe) was oxidized in air, the product was a single phase of MgFe<sub>2</sub>O<sub>4</sub>, as shown in Fig. 2. Therefore, the reduced MgFe<sub>2</sub>O<sub>4</sub> (MgO/Fe) reacts with oxygen in air to induce the oxidation reaction as follows.



Fe could only be oxidized to Fe<sub>3</sub>O<sub>4</sub> under steam. In the steam reactor, the reduced MgFe<sub>2</sub>O<sub>4</sub> (MgO/Fe) reacts with H<sub>2</sub>O to induce the oxidation reaction as follows.



Meanwhile, when the sample oxidized in the steam reactor goes into the air reactor, MgO and Fe<sub>3</sub>O<sub>4</sub> become fully re-oxidized by oxygen and form the single phase of MgFe<sub>2</sub>O<sub>4</sub> as follows.



### Oxygen transfer properties of MgFe<sub>2</sub>O<sub>4</sub>

The redox cycle curves obtained using TGA at 900 °C with 5% H<sub>2</sub>/N<sub>2</sub> and air used as reducing and oxidizing gases, respectively, during three redox cycles

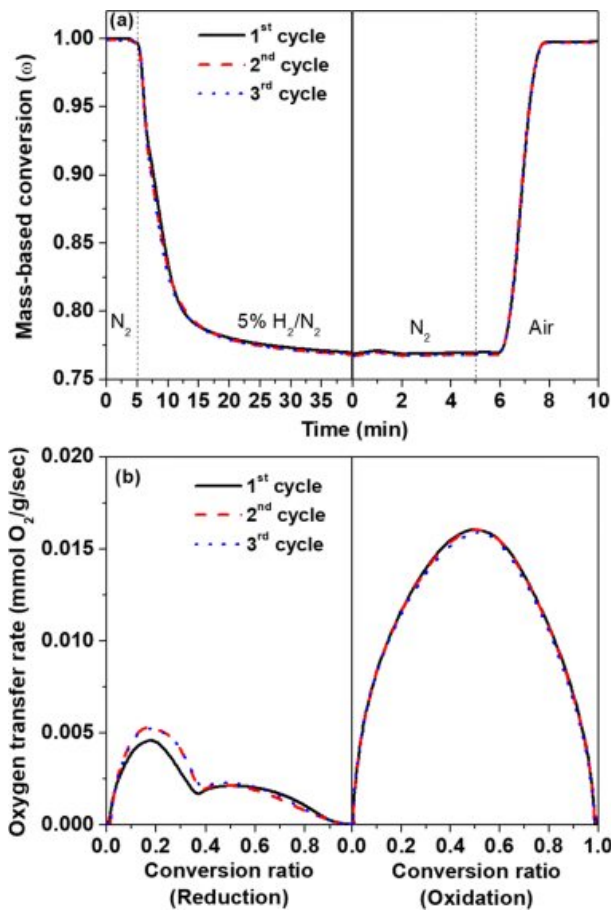


**Fig. 4.** (a) Redox cycle curves and (b) oxygen transfer rate of  $MgFe_2O_4$  at 900 °C with 5%  $H_2/N_2$  and air used as the reducing and oxidizing gases, respectively; measured by TGA.

are shown in Fig. 4(a). When oxidized by air, the weight gain is equal to the weight loss during reduction. This indicates that the redox reaction between  $MgFe_2O_4$  and  $MgO/Fe$ , based on equation (4) and equation (7), is reversible. This reversible redox reaction can also be confirmed by the phase analysis, as shown in Fig. 1 and Fig. 2. While the oxidation reaction was completed within 8 min after the oxidizing gas was introduced, the reduction reaction takes over 40 min. The oxygen transfer rate, which is the amount of oxygen consumed per unit time and weight [mmol- $O_2/g/s$ ], can be calculated from TGA data (Fig. 4(a)). The oxygen transfer rate for the oxidation reaction was clearly noted to be about three times as fast as that for the reduction reaction, as shown in Fig. 4(b). Nam et al. reported similar results, where that reaction rate of air oxidation was much faster than that of  $CH_4$  reduction for an  $Fe_2O_3/ZrO_2$  oxygen carrier material [23]. The obtained activation energies of reduction by  $CH_4$  and oxidation by air at 900 °C were 219 and 20 kJ/mol, respectively [23].

With the 5%  $CO/N_2$  fuel, a similar trend for the redox cycle curves and the oxygen transfer rate was observed, as shown in Fig. 5. In particular, the oxidation

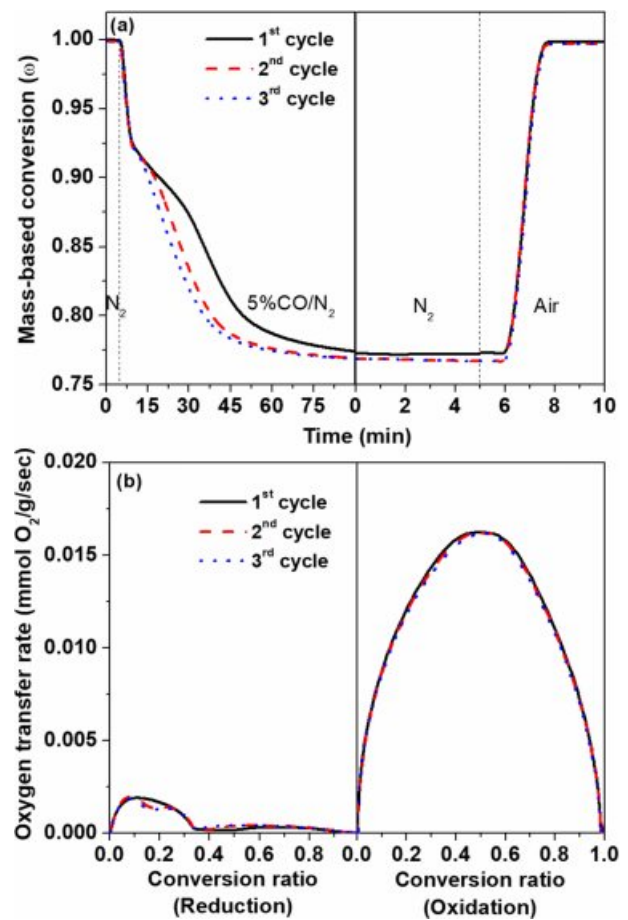


**Fig. 5.** (a) Redox cycle curves and (b) oxygen transfer rate of  $MgFe_2O_4$  at 900 °C with 5%  $CO/N_2$  and air used as the reducing and oxidizing gases, respectively; measured by TGA.

curve and oxygen transfer rate of oxidation in Figs. 4 and 5 are identical. This indicates that the oxidation mechanism based on equation (7) is favorable. However, the oxygen transfer rate of reduction for 5%  $CO/N_2$  is much slower compared to that for 5%  $H_2/N_2$ . It has been reported that the chemical kinetic constant,  $K_s$ , for the reaction of  $H_2$  with  $Fe_2O_3/Al_2O_3$  oxygen carriers is significantly larger than that of  $CO$ , and the activation energies for the reaction of  $H_2$  and  $CO$  are 8 and 14 kJ/mol, respectively [24].

Fig. 6 shows the change of the microstructure due to the reducing gas at the first redox cycle. The as-synthesized  $MgFe_2O_4$  powder has a small granular surface with necking between particles. The  $MgFe_2O_4$  powder reduced in 5%  $H_2/N_2$  at 900 °C, which is  $MgO/Fe$ , has a porous structure with smaller particles, as compared with the initial  $MgFe_2O_4$  powder; this is due to the loss of oxygen and recombination of cations during the reduction reaction. Alternatively, the  $MgFe_2O_4$  powder reduced in 5%  $CO/N_2$  at 900 °C shows significant grain growth. In the case of the sample reduced by 5%  $CO/N_2$ , the sample has remained at a high temperature for a long time for complete reduction to  $MgO/Fe$ , as

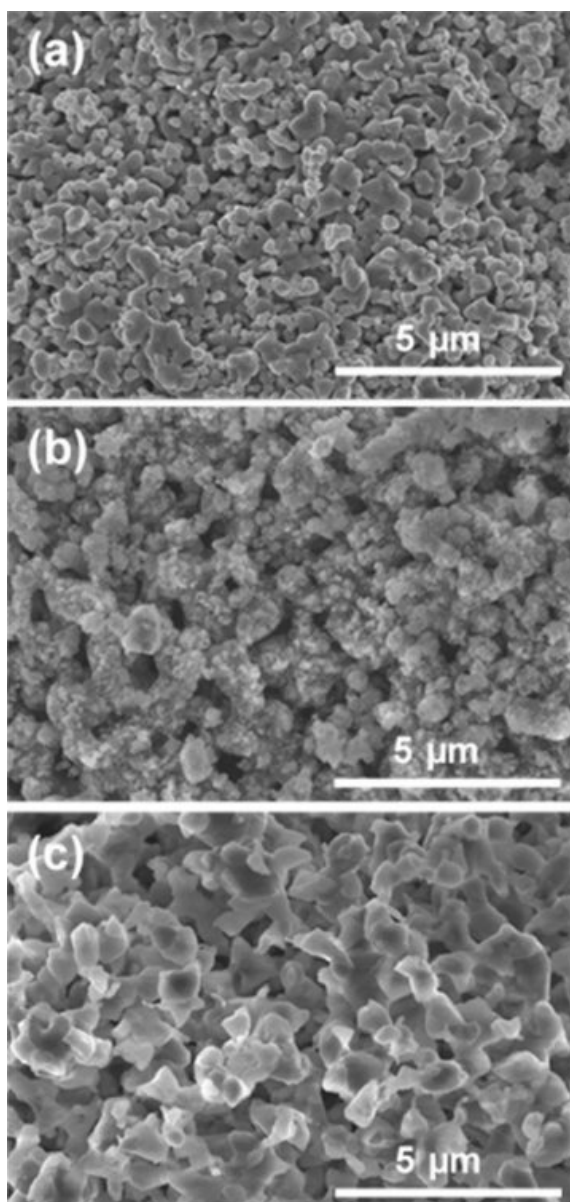


**Fig. 6.** FE-SEM images of  $\text{MgFe}_2\text{O}_4$ : (a) as-synthesized and reduced by (b) 5%  $\text{H}_2/\text{N}_2$  and (c) 5%  $\text{CO}/\text{N}_2$  at 900 °C.

shown in Fig 5(a). Therefore, a lot of grain growth has occurred.

The calculated oxygen transfer capacities and maximum oxygen transfer rates of  $\text{MgFe}_2\text{O}_4$  at 900 °C with different reducing gases according to the redox cycle number are shown in Fig. 7. The average oxygen transfer capacities of  $\text{MgFe}_2\text{O}_4$  for 5%  $\text{H}_2/\text{N}_2$  and 5%  $\text{CO}/\text{N}_2$  gases during 10 redox cycles were 23.2 and 23.0 wt%, respectively. The empirical oxygen transfer capacities of  $\text{MgFe}_2\text{O}_4$  were similar to the theoretical value of 24.0 wt%, based on equation (4) and equation (5). Moreover, no degradation of the oxygen transfer capacity or maximum transfer rate was observed during the redox cycles. Generally, the oxygen transfer capacity and rate decrease with increasing redox cycle number when an irreversible

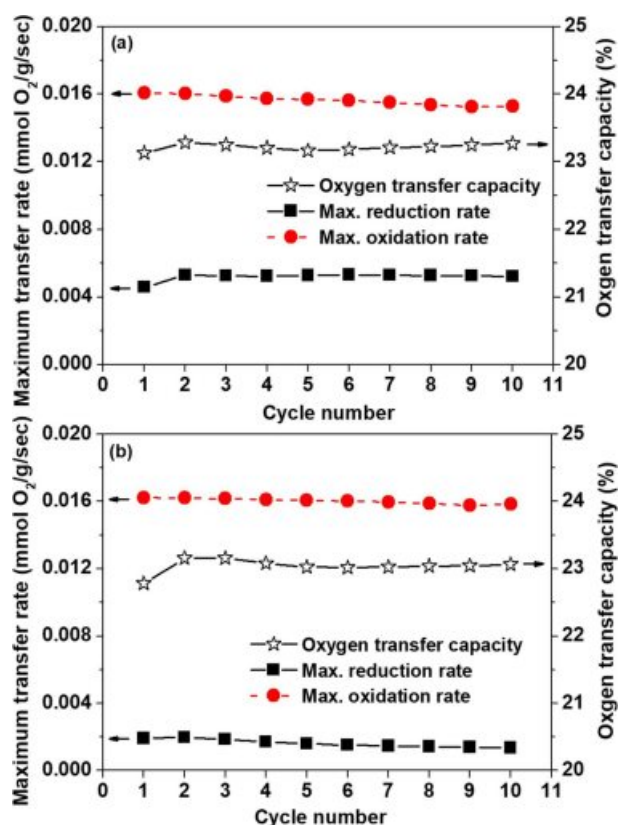


**Fig. 7.** Variation of oxygen transfer capacity and maximum oxygen transfer rate of  $\text{MgFe}_2\text{O}_4$  at 900 °C according to the redox cycle number for (a) 5%  $\text{H}_2/\text{N}_2$  and (b) 5%  $\text{CO}/\text{N}_2$  gases; measured by TGA.

phase transition occurs. Since the redox reaction of  $\text{MgFe}_2\text{O}_4$  was reversible, as shown in Fig. 2,  $\text{MgFe}_2\text{O}_4$  maintained its phase and crystal structure after redox cycling; this demonstrates the material's good oxygen carrier stability.

The microstructure of  $\text{MgFe}_2\text{O}_4$  before cycling and after the 10th redox cycle is shown in Fig. 8. Unlike other Fe-based oxygen carrier materials, such as  $\text{Fe}_2\text{O}_3$  [25], no agglomeration was observed after redox cycling, regardless of the reducing gases. In general, when agglomeration occurs, the specific surface area of the oxygen carrier material decreases; this leads to a decrease in the reactivity. Therefore, the microstructural stability and the phase stability during redox cycling might explain why  $\text{MgFe}_2\text{O}_4$  showed excellent oxygen carrier stability (Fig. 7). Alternatively, the sample using 5%  $\text{CO}/\text{N}_2$  as the reducing gas was observed to be more fragile. Attrition is an important property of oxygen carrier materials in the case of fluidized bed reactors. Attrition can also act as an indicator of whether an oxygen carrier material is capable of undergoing a reaction without any loss of particles [26]. In this regard, further research on ways to improve the attrition resistance of  $\text{MgFe}_2\text{O}_4$  should be undertaken; for example, the addition of an inorganic binder such as  $\text{Al}_2\text{O}_3$ ,  $\text{ZrO}_2$ ,  $\text{CeO}_2$  could be beneficial [27, 28].

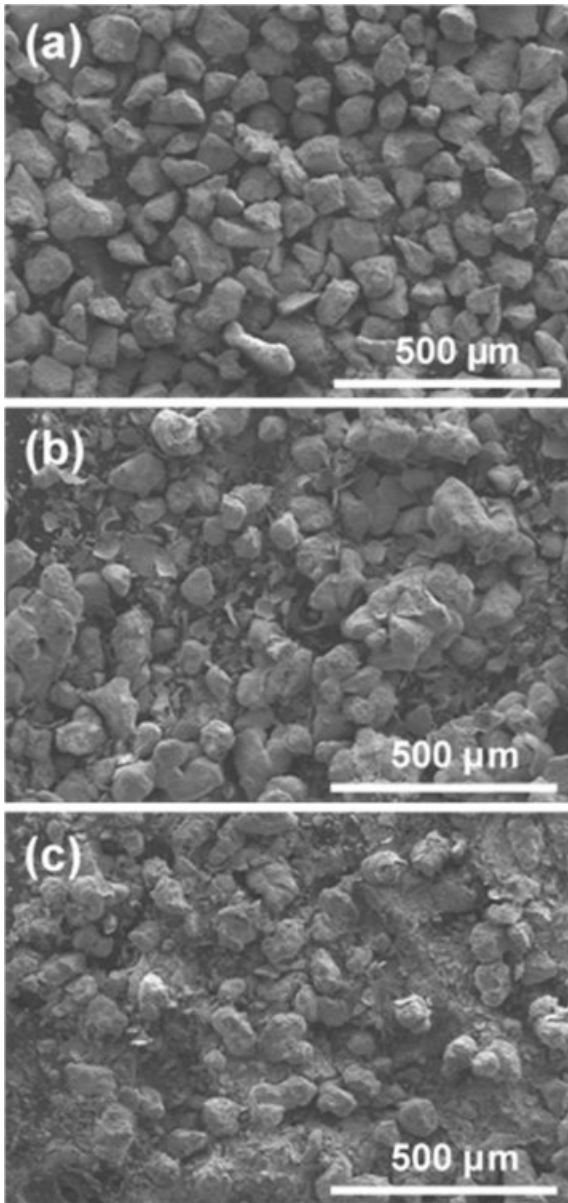


**Fig. 8.** FE-SEM images of  $\text{MgFe}_2\text{O}_4$ : (a) before cycling and after the 10th redox cycle at  $900^\circ\text{C}$  with (b) 5%  $\text{H}_2/\text{N}_2$  and (c) 5%  $\text{CO}/\text{N}_2$  reducing gases.

### $\text{H}_2$ production behavior of $\text{MgFe}_2\text{O}_4$

The  $\text{H}_2$  production behavior of  $\text{MgFe}_2\text{O}_4$  was analyzed by GC during redox cycling using 5%  $\text{H}_2/\text{Ar}$  for reduction and 10%  $\text{H}_2\text{O}/\text{Ar}$  for oxidation at  $900^\circ\text{C}$ . Fig. 9(a) shows the variation of the  $\text{H}_2$  concentration during four redox cycles. The calculated  $\text{H}_2$  production amount and maximum production rate for the oxidation reaction are shown in Fig. 9(b). The  $\text{H}_2$  concentration during the reduction and oxidation reactions, respectively, remained constant during redox cycling. This indicates that the reversible reaction based on equation (8) occurs ( $\text{MgO}/\text{Fe} \leftrightarrow \text{MgO}/\text{Fe}_3\text{O}_4$ ). Conversely, for the redox reaction using 5%  $\text{H}_2/\text{N}_2$  for reduction and air for oxidation, the solid phase changes between  $\text{MgO}/\text{Fe}$  and  $\text{MgFe}_2\text{O}_4$ .

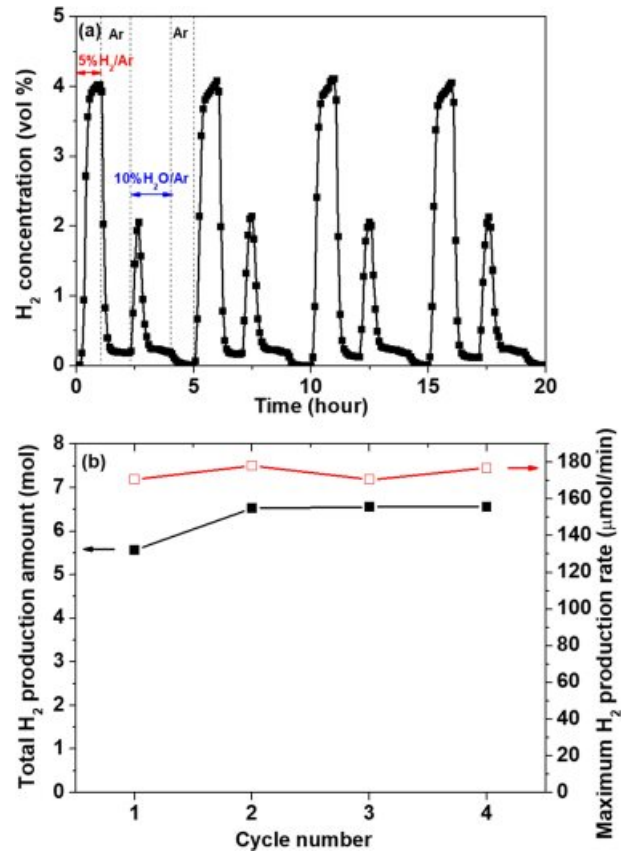


**Fig. 9.** (a) Variation of the  $\text{H}_2$  concentration of  $\text{MgFe}_2\text{O}_4$  with 5%  $\text{H}_2/\text{Ar}$  and 10%  $\text{H}_2\text{O}/\text{Ar}$  as the reducing and oxidizing gases, respectively, during four redox cycles measured by GC at  $900^\circ\text{C}$ , and (b) the calculated  $\text{H}_2$  production and maximum  $\text{H}_2$  production rate according to the redox cycle number.

Importantly,  $\text{MgFe}_2\text{O}_4$  showed no significant degradation in terms of the calculated  $\text{H}_2$  production and maximum production rate, as shown in Fig. 9(b). Assuming that the reaction rate of  $\text{H}_2$  production per minute is maintained, the average amount of  $\text{H}_2$  production for  $\text{MgFe}_2\text{O}_4$  would be 2,806 L/day per unit mass (kg).

### Conclusions

The present study investigated  $\text{MgFe}_2\text{O}_4$  spinel as an innovative oxygen carrier material for CLHP.  $\text{MgFe}_2\text{O}_4$  reacts with various gases, such as  $\text{H}_2$ ,  $\text{CO}$ , and  $\text{CH}_4$ , and is reduced to  $\text{MgO}$  and  $\text{Fe}$ . The solid-state redox pathways in the fuel, steam, and air reactors are  $\text{MgFe}_2\text{O}_4 \rightarrow \text{MgO}/\text{Fe}$ ,  $\text{MgO}/\text{Fe} \rightarrow \text{MgO}/\text{Fe}_3\text{O}_4$ , and  $\text{MgO}/\text{Fe}_3\text{O}_4 \rightarrow \text{MgFe}_2\text{O}_4$ , respectively. The oxygen transfer capacity of  $\text{MgFe}_2\text{O}_4$  was found to be 23 wt% when it was fully reduced to  $\text{MgO}/\text{Fe}$ ; this is similar to the theoretical value of 24 wt%. The oxygen transfer capacity and rate were maintained during 10 redox cycles because  $\text{MgFe}_2\text{O}_4$  does not show any phase or crystal structure changes or agglomeration. Similarly, both the total amount and the maximum rate of  $\text{H}_2$  production for  $\text{MgFe}_2\text{O}_4$  were maintained without significant degradation

during four redox cycles. In this regard,  $MgFe_2O_4$  represents a promising oxygen carrier material for CLHP due to its stability and high performance. However, although  $MgFe_2O_4$  shows good oxygen transfer properties and  $H_2$  production behavior, it also showed problems related to attrition resistance. Therefore, a new approach to improve the attrition resistance of  $MgFe_2O_4$ , such as the addition of an inorganic binder, should be further investigated.

### Acknowledgements

This research was supported by Basic Science Research Program through the National Research Foundation of Korea (NRF) funded by the Ministry of Education (2017R1D1A1B03031541). This work was also supported by the National Research Foundation of Korea (NRF) grant funded by the Korea government (MSIT) (No. 2018R1A4A1025528).

### References

1. International Energy Outlook, (2017) <<https://www.eia.gov/outlooks/ieo>>.
2. IPCC, in 2014: Climate Change 2014: Synthesis Report, 2015, edited by R.K. Pachauri, and L.A. Meyer, Intergovernmental Panel on Climate Change Press (2015) p.151.
3. K. Go, S. Son, S. Kim, K. Kang, and C. Park, *Int. J. Hydrogen Energy* 34[3] (2009) 1301-1309.
4. R. Solunke and G. Veser, *Ind. Eng. Chem. Res.* 49[21] (2010) 11037-11044.
5. M. El-Shafie, S. Kambara, and Y. Hayakawa, *J. Power Energy Eng.* 7 (2019) 107-154.
6. J.P.V. Hook, *Catal. Rev.* 21 (1980) 1-51.
7. M.N. Khan and T. Shamim, *Energy Procedia* 61 (2014) 2034-2037.
8. B. Li, Y. Duan, D. Luebke, and B. Morreale, *Appl. Energy* 102 (2013) 1439-1447.
9. L.-S. Fan, L. Zeng, W. Wang, and S. Luo, *Energy Environ. Sci.* 5 (2012) 7254-7280.
10. F.X. Li, H.R. Kim, D. Sridhar, F. Wang, and L. Zeng, J. Chen, L.S. Fan, *Energy Fuels* 23[8] (2009) 4182-4189.
11. Z. Huang, F. He, Y. Feng, K. Zhao, A. Zheng, S. Chang, G. Wei, Z. Zhao, and H. Li, *Energy Fuels* 28[1] (2014), 183-191.
12. P. Chies, G. Lozza, A. Malandrino, M. Romano, and V. Piccolo, *Int. J. Hydrogen Energy* 33 (2008), 2233-2245.
13. B.S. Kwak, N.-K. Park, S.O. Ryu, J.-I. Baek, H.-J. Ryu, and M. Kang, *Chem. Eng.* 309 (2017) 617-627.
14. M.M. Tijani, A. Aqsha, and N. Mahinpey, *Energy* 138 (2017) 873-882.
15. J.H. Hwang, K.T. Lee, *J. Ceram. Proc. Res.* 20[1] (2019) 18-23.
16. P. Gupta, L.G. Velazquez-Vargas, and L.S. Fan, *Energy Fuels* 21[5] (2007) 2900-2908.
17. M. Rydén, E. Cleverstam, M. Johansson, A. Lyngfelt, and T. Mattisson, *AIChE J.* 56 (2010) 2211-2220.
18. Z. Huang, F. He, Y. Feng, K. Zhao, A. Zheng, S. Chang, G. Wei, Z. Zhao, and H. Li, *Energy Fuels* 28[1] (2014) 183-191.
19. S. Yang, K. Kim, J.I. Baek, J.W. Kim, J.B. Lee, C.K. Ryu, and G. Lee, *Energy Fuels* 26[7] (2012) 4617-4622.
20. S. Liu, F. He, Z. Huang, A. Zheng, Y. Feng, Y. Shen, H. Li, H. Wu, and P. Glarborg, *Energy Fuels* 30 (2016) 4151-4262.
21. Y.-C. Liu, Y. Ku, Y.-H. Tseng, H.-Y. Lee, and Y.-L. Kuo, *Aerosol Air Qual. Res.* 16 (2016) 2023-2032.
22. T. Yamashita and P. Hayes, *Appl. Surf. Sci.* 254 (2008) 2441-2449.
23. H. Nam, K. Kang, K. Bae, C. Kim, W. Cho, Y. Kim, and C. Park, *Trans. Korean Hydrog. New Energy Soc.* 22[2] (2011) 168-177.
24. A. Cabello, A. Abad, F. García-Labiano, P. Gayán, L.F. de Diego, and J. Adánez, *Chem. Eng. J.* 258 (2014) 265-280.
25. M. Zhu, Y. Song, S. Chen, M. Li, L. Zhang, and W. Xiang, *Chem. Eng. J.* 368 (2019) 812-823.
26. S. Sajen, S.K. Singh, G. Saravanan, A.H. Fakeeha, A.S. Al-Fateh, A.A. Ibrahim, M.A. Amrani, A.B. Mahindrakar, and N. Labhsetwar, *J. Energy Environ. Sustain.* 5 (2018) 30-40.
27. T. Mattisson, J. Adánez, K. Mayer, F. Snijders, G. Williams, E. Wesker, O. Bertsch, and A. Lyngfelt, *Energy Procedia* 63 (2014) 113-130.
28. M. Rydén, P. Moldenhauer, S. Lindqvist, T. Mattisson, and A. Lyngfelt, *Powder Tech.* 256 (2014) 75-86.